Published in final edited form as:
Nature. 2011 January 20; 469(7330): 402–406. doi:10.1038/nature09600.

Development of asymmetric inhibition underlying direction selectivity in the retina

Wei Wei[1], **Aaron M. Hamby**[1], **Kaili Zhou**[1], and **Marla B. Feller**[1,2]

[1]Department of Molecular & Cell Biology, University of California, Berkeley, California 94720-3200, USA

[2]Helen Wills Neurosciences Institute, University of California, Berkeley, California 94720-3200, USA

Abstract

Establishing precise synaptic connections is crucial to the development of functional neural circuits. The direction-selective circuit in the retina relies upon highly selective wiring of inhibitory inputs from starburst amacrine cells[1] (SACs) onto four subtypes of on–off direction-selective ganglion cell (DSGC), each preferring motion in one of four cardinal directions[2]. It has been reported in rabbit that the SACs on the 'null' sides of DSGCs form functional GABA (γ-aminobutyric acid)-mediated synapses, whereas those on the preferred sides do not[3]. However, it is not known how the asymmetric wiring between SACs and DSGCs is established during development. Here we report that in transgenic mice with cell-type-specific labelling, the synaptic connections from SACs to DSGCs were of equal strength during the first postnatal week, regardless of whether the SAC was located on the preferred or null side of the DSGC. However, by the end of the second postnatal week, the strength of the synapses made from SACs on the null side of a DSGC significantly increased whereas those made from SACs located on the preferred side remained constant. Blocking retinal activity by intraocular injections of muscimol or gabazine during this period did not alter the development of direction selectivity. Hence, the asymmetric inhibition between the SACs and DSGCs is achieved by a developmental program that specifically strengthens the GABA-mediated inputs from SACs located on the null side, in a manner not dependent on neural activity.

The ability to detect motion in the visual scene is a fundamental computation in the visual system that is first performed in the retina. Motion direction is encoded by DSGCs, which fire a maximum number of action potentials during movement in their preferred direction, but fire minimally for movement in the opposite, or null, direction[4,5]. In the mammalian retina, the directional preference of an on–off DSGC is caused by asymmetric inhibitory inputs: movement in the null direction causes strong inhibition that effectively shunts light-evoked excitatory inputs. Indeed, blocking $GABA_A$ receptors abolishes the directionality of DSGCs by increasing spiking in response to null-direction motion[6–8]. Null-side inhibition is

Correspondence and requests for materials should be addressed to M.B.F. (mfeller@berkeley.edu).

Supplementary Information is linked to the online version of the paper at www.nature.com/nature.

Author Contributions W.W. conducted the electrophysiology and imaging experiments, and manuscript preparation; A.M.H. conducted intraocular injections, verification of the injection method and activity blockade, and manuscript preparation. K.Z. conducted NEUROLUCIDA reconstructions and analysis. M.B.F. was involved in the experimental design, data analysis of Supplementary Fig 3c–e and manuscript preparation.

The authors declare no competing financial interests.

Readers are welcome to comment on the online version of this article at www.nature.com/nature.

thought to arise from SACs because their processes cofasciculate with DSGC dendrites[9,10], where they form direct GABAergic synapses[3], and because ablation of SACs eliminates the directional preference of DSGCs[11,12].

How SAC–DSGC synapses are organized to provide asymmetric inhibition has been an intriguing but difficult question because no apparent asymmetry is detected in the morphology or the distribution of synaptic markers in DSGCs and SACs[13–15]. The first and only piece of evidence for the synaptic basis of asymmetric inhibition came from a functional study between SAC and DSGC pairs in rabbit retina[3], which suggested that SACs on the null side provide inhibitory inputs to the DSGCs but that those on the preferred side do not. Whether this asymmetric inhibition exists in the mouse is not known. In addition, because the directional preference of an on–off DSGC is present by eye opening[16–18] and the identification of DSGCs and their preferred directions is almost impossible before the onset of the light response, little is known about the developmental program that shapes the SAC–DSGC synapses.

Here we use paired recordings and morphological reconstructions from a double-transgenic mouse line that selectively expresses two variants of green fluorescent protein (GFP) in SACs and nasal-preferring on–off DSGCs (nDSGCs) to characterize the organization and the development of the precise wiring between SACs and DSGCs. These mice were generated by crossing two existing lines: *Drd4–GFP* mice, where *Drd4* promoter-driven GFP expression is restricted to nDSGCs[19], and *mGluR2–GFP* mice (*mGluR2* also known as *Grm2*), where a membrane-tethered human interleukin-2α/GFP fusion protein is expressed specifically in SACs in the retina (Fig. 1a)[20].

To detect functional GABAergic synapses between SACs and DSGCs, we performed targeted whole-cell voltage-clamp recordings from SAC–DSGC pairs in whole-mount retinas. To isolate GABAergic synapses, paired recordings were carried out in the presence of drugs that block excitatory synaptic transmission (Fig. 1b). Alexa dyes were included in the recording pipettes to visualize the dendritic morphology of the recorded pairs (Fig. 1c). Only pairs with overlapping dendritic fields were used for analysis.

Paired recordings were carried out in postnatal-day-4 (P4), P7, P14 and adult mice. At P4, GABAergic currents elicited by SAC depolarization were detected in nDSGCs in 64% of pairs (16 of 25 pairs; Fig. 1b, d), indicating that synapse formation between SACs and nDSGCs occurred before and during the first postnatal week, confirming previous findings[10]. By P7, nearly all pairs showed unitary GABAergic connections (P7: 85%, 29 of 34 pairs), and this high level of connectivity persisted into adulthood (P14–48: 91%, 41 of 45 pairs; Fig. 1d). The evoked response was completely blocked by the $GABA_A$ receptor antagonist gabazine (5 μM, $n = 4$; data not shown), indicating that the GABAergic transmission between SACs and nDSGCs is mediated by $GABA_A$ receptors. We note that the finding that connections were readily detected between SACs located on the preferred side of DSGCs in adult mice is in contrast to previous findings in rabbit[3].

Though SACs located on both the preferred side and the null side formed GABAergic synapses with DSGCs, a significant asymmetry in the unitary synaptic strength emerged along the null-preferred axis during the second postnatal week. Synaptic strength was quantified as the $GABA_A$-receptor-mediated whole-cell conductance. These measurements were conducted from the null-side and preferred-side pairs that had similar amounts of overlap between SAC processes and DSGC dendrites. Unexpectedly, at P4 and P7 the GABAergic conductances from both groups were similar (Fig. 2). However, a significant increase in unitary conductance was detected in the null-side pairs but not in the preferred side pairs in retinas at P14 and older (Fig. 2). Hence, the establishment of the direction-

selective circuits is mediated by an asymmetric increase in the strength of the unitary conductance between SACs and DSGCs in the week before eye opening.

The difference in GABAergic conductance from the null- and preferred-side SACs prompted us to examine two possibilities regarding the mechanisms underlying this strengthening. First we tested whether this functional asymmetry was correlated with the number or quality of contacts between SACs and nDSGCs, indicating a preferential adhesion between SACs located on the null side and DSGCs[3], which is an important mechanism for dendritic differentiation and synaptogenesis in other systems[21,22]. After electrophysiological recording, the dendritic arborizations of the synaptically connected, Alexa-dye-filled SAC–nDSGC pairs from P14 to P48 were imaged live with a two-photon microscope and reconstructed using NEUROLUCIDA (Fig. 3a). We examined the overlapping region between the nDSGC dendrites and the distal portion (roughly the outer third) of the SAC processes enriched in varicosities, which are the sites of neurotransmitter release[9]. Crossing points between distal SAC processes and nDSGC dendrites were defined as 'contacts' (Fig. 3a, inset). A subset of contacts exhibited cofasciculation[9,10,23], which were defined as 2-μm segments along which the processes from the two cells remained in contact (Fig. 3a, inset). The null- and preferred-side SAC–nDSGC pairs showed a similar density of contacts (Fig. 3b) and cofasciculations (Fig. 3c). No asymmetry was found when all of the SAC processes were included in the above analysis (Supplementary Fig. 1). Therefore, the functional asymmetry in GABAergic synapses does not involve selective adhesion between null-side SAC processes and DSGC dendrites[24].

The second possibility we tested was whether spontaneous retinal activity during the second postnatal week had a role in the establishment of direction selectivity. DSGCs are depolarized by retinal waves, and activity could therefore potentially influence the synapse strengthening[25]. To this end, we first confirmed that the GFP-labelled nDSGCs in the *Drd4–GFP* mice showed a clear preference for nasal motion at eye opening (Fig. 4a) that was sensitive to the $GABA_A$ receptor antagonist gabazine (Supplementary Fig. 2), with a direction selectivity index similar to those recorded in the adult (Fig. 4b). We then injected muscimol, a $GABA_A$ receptor agonist, intravitreally into *Drd4–GFP* mice to block all spontaneous and evoked neural activity in the retina[26]. In the presence of muscimol, evoked synaptic transmission from SACs to nDSGCs and spontaneous activity in both cell types were completely suppressed (Fig. 4c and Supplementary Fig. 3a, b). The effectiveness of muscimol injection at blocking activity *in vivo* was confirmed by examining eye-specific segregation of retinogeniculate projections, which is an independent measure of retinal activity (Supplementary Fig. 3c, d), and the persistence of fluorescently labelled muscimol in the retina at 48 h post-injection (Supplementary Fig. 3e).

We assessed the responses of nDSGCs to stationary flashes and drifting gratings in P14–15 mice that had received repeated muscimol injections in the second postnatal week. Muscimol treatment did not prevent the development of direction-selective responses or significantly reduce directional tuning of nDSGCs (Fig. 4a, b). Normal on and off light responses were also present in the muscimol-treated group, although there was an increase in the number of cells that did not respond to gratings in the muscimol-treated group (Supplementary Fig. 4).

In visual cortex, activation of $GABA_A$ receptors is required for maturation of GABAergic synapses[27]. To test the hypothesis that $GABA_A$ receptor activation is required for the development of direction selectivity, we performed intravitreal injections of the $GABA_A$ receptor antagonist gabazine into *Drd4–GFP* mice during the second postnatal week. Gabazine treatment did not prevent the development of direction-selective responses of

GFP-positive cells to drifting gratings (Fig. 4a, b). Therefore, the development of direction selectivity arises independently of the activation of $GABA_A$ receptors.

To begin exploring the synaptic basis of this increase in conductance between null-side SACs and DSGCs, we recorded the spontaneous inhibitory postsynaptic currents (IPSCs) from nDSGCs at P7 and P14. We found a significant increase in the frequency and no significant change in the amplitude of the GABAergic IPSCs, although there was a trend towards larger IPSC amplitudes at P14 (Supplementary Fig. 5). This result is consistent with the hypothesis that the stronger GABAergic unitary conductance for the null-side pairs is primarily due to increased numbers of functional GABAergic synapses. However, we cannot tell whether the spontaneous IPSCs originate from the null- or preferred-side SACs. Further study is required to determine the relative role increases in synapse number versus synapse strength have in the increase in the unitary conductance between null-side SAC and DSGCs.

Our study demonstrates that asymmetric inhibition arises during the second postnatal week through selective strengthening of the GABAergic conductance from SACs on the null sides of DSGCs. Morphological analysis revealed a similar degree of dendritic contact and cofasciculation between SACs on the null or preferred side, indicating that the synapse development is dissociated from physical encounters between SAC processes and DSGC dendrites, as was recently found in barrel cortex[28].

In addition, we found that blocking depolarization-induced activity or $GABA_A$ receptor activation did not affect the establishment of direction selectivity in the retina, in sharp contrast to direction-selective cells in the visual cortex[29]. This finding lends support to previous studies showing that early visual experience[16–18] or cholinergic retinal waves[18] are not involved in establishing retinal direction selectivity. Therefore, the mechanism underlying the development of retinal direction selectivity is an asymmetric increase in the strength of the inhibitory unitary conductance between SACs and DSGCs in the week before eye opening, without the establishment of asymmetrical dendritic contacts and independent of spontaneous neural activity.

METHODS

Mice

Drd4–GFP mice in the Swiss Webster background were obtained from MMRRC[19] (http://www.mmrrc.org/strains/231/0231.html), and *mGluR2–GFP* mice were a gift from Shigatada Nakanishi, Osaka. Both strains were backcrossed to the C57BL/6 background in our laboratory. The *Drd4–GFP*/*mGluR2–GFP* double-transgenic mice were obtained by crossing the two single-transgenic lines.

Whole-cell patch-clamp recording

Single or dual whole-cell voltage-clamp recordings from SACs and nDSGCs were performed in oxygenated artificial cerebrospinal fluid at 32–34 °C containing 119.0 mM NaCl, 26.2 mM $NaHCO_3$, 11 mM glucose, 2.5 mM KCl, 1.0 mM K_2HPO_4, 2.5 mM $CaCl_2$, 1.3 mM $MgCl_2$, 0.05 mM AP5, 0.02 mM DNQX and 0.008 mM DHβE. Recording electrodes of 3–5 MΩ were filled with an internal solution containing 110 mM $CsMeSO_4$, 2.8 mM NaCl, 4 mM EGTA, 5 mM TEA-Cl, 4 mM adenosine 5′-triphosphate (magnesium salt), 0.3 mM guanosine 5′-triphosphate (trisodium salt), 20 mM HEPES and 10 mM phosphocreatine (disodium salt), 0.025 mM Alexa 488 (for SACs) and 0.025 mM Alexa 594 (for nDSGCs), pH 7.25. Data were acquired using PCLAMP 10 recording software and a Multiclamp 700A amplifier (Molecular Devices), filtered at 4 kHz and digitized at a sampling rate of 10 kHz. The GABAergic whole-cell conductance was calculated from the

linear portion of the current–voltage curve for the SAC-evoked currents in nDSGCs and analysed using MATLAB software.

Two-photon targeted loose-patch recording of *GFP*-positive neurons for light response

Drd4–GFP mice were anaesthetized with isofluorane and decapitated in accordance with the UC Berkeley Institutional Animal Care and Use Committee and in conformance with the NIH Guide for the Care and Use of Laboratory Animals, the Public Health Service Policy and the SFN Policy on the Use of Animals in Neuroscience Research. Under infrared illumination, retinas were isolated from the pigment epithelium in oxygenated Ames' medium (Sigma), cut into dorsal and ventral halves, and mounted over a hole of 1–1.5 mm^2 on filter paper (Millipore) with the photoreceptor layer facing down. Retinas were kept in darkness at room temperature in Ames' medium bubbled with 95% O2/5% CO2 until use (0–7 h). Recording electrodes of 3–5 MΩ were filled with Ames' medium. GFP fluorescence was detected with a custom-built, FluoView-based two-photon microscope and a Ti:sapphire laser (Coherent) tuned to 920 nm, a wavelength that minimally activates mouse photoreceptors and therefore preserves light response. GFP cells were then targeted for loose-patch recordings using PCLAMP 10 recording software and a Multiclamp 700A amplifier.

Visual stimuli were generated as previously described[19]. Briefly, a white, monochromatic organic light-emitting display (OLEDXL, eMagin; 800 × 600 pixel resolution, 85-Hz refresh rate) was controlled by an Intel Core Duo computer with a Windows XP operating system. Drifting square-wave gratings (spatial frequency, 225 mm per cycle; temporal frequency, 4 cycles s^{-1}; 30° s^{-1} in 12 pseudorandomly chosen directions spaced at 30 intervals, with each presentation lasting 3 s and followed by 500 ms of grey screen) were generated from the OLED using MATLAB and the Psychophysics Toolbox, and were projected through the ×60 water-immersion objective (LUMPlanFl/IR, NA 0.9) via the side port of the microscope, centred on the soma of the recorded cell and focused on the photoreceptor layer. Loose-patch recordings were obtained during the stimulus presentation and analysed using MATLAB. A detailed, step-by-step protocol of the two-photon targeted recording of light response can be found in ref. 30.

Two-photon microscopy and morphological reconstruction

After paired recording, the Alexa-488-filled SACs and the Alexa-594-filled nDSGCs in the *Drd4–GFP*/*mGluR2–GFP* mice were imaged using the two-photon microscope at 745 nm. At this wavelength, GFP is not efficiently excited but both Alexa 488 and Alexa 594 are brightly fluorescent. Therefore, the morphology of the Alexa-488-filled SACs could be distinguished from the very weak GFP fluorescence. Image stacks were acquired at *z* intervals of 0.5 μm and resampled three times for each stack using a ×60 objective (Olympus LUMPlanFl/IR ×60/0.90W), covering the entire dendritic fields of the SACs and nDSGCs. Image stacks from 25 SAC–nDSGC pairs were then imported into NEUROLUCIDA (MBF Biosciences) and reconstructed in three dimensions. The densities of contacts and cofasciculations were measured from the reconstructions.

Intraocular injections

Drd4–GFP animals were anaesthetized with 3.5% isoflurane/2% O_2. The eyelid was then opened with fine forceps, and 1 μl of 10 mM muscimol (Tocris), 500 μM gabazine (Tocris) or saline was injected using a fine glass micropipette. Injections were made with a picospritzer (World Precision Instruments) generating 20-p.s.i., 3-ms-long positive pressure. To prevent efflux of the injected solution, removal of the pipette tip from the eye was done slowly and gentle pressure was then applied to the injection site with a sterile cotton swab for ~10 s. This procedure was repeated every 48 h, starting at P6 and ending at P12.

Statistical analysis

Grouped data are presented as mean ± s.d. or s.e. as indicated. Data sets were tested for normality, and statistical differences were examined using one-way analysis of variance and *post hoc* comparisons using Student's *t*-test with Bonferroni corrections (MATLAB).

Supplementary Material

Refer to Web version on PubMed Central for supplementary material.

Acknowledgments

We thank [AUTHOR: our house style does not allow for affiliations in Acknowledgements.] S. Nakanishi for *mGluR2–GFP* mice, A. Huberman for *Drd4–GFP* mice, J. Elstrott for help with MATLAB software, P. Han for mouse genotyping, J. Ledue for imaging assistance and A. Blankenship for reading the manuscript. This work was supported by grants RO1EY013528 and ARRA EY019498 from the National Institutes of Health.

References

1. Euler T, Detwiler PB, Denk W. Directionally selective calcium signals in dendrites of starburst amacrine cells. Nature. 2002; 418:845–852. [PubMed: 12192402]
2. Demb JB. Cellular mechanisms for direction selectivity in the retina. Neuron. 2007; 55:179–186. [PubMed: 17640521]
3. Fried SI, Munch TA, Werblin FS. Mechanisms and circuitry underlying directional selectivity in the retina. Nature. 2002; 420:411–414. [PubMed: 12459782]
4. Barlow HB, Levick WR. The mechanism of directionally selective units in rabbit's retina. J Physiol (Lond). 1965; 178:477–504. [PubMed: 5827909]
5. Oyster CW. The analysis of image motion by the rabbit retina. J Physiol (Lond). 1968; 199:613–635. [PubMed: 5710424]
6. Ariel M, Daw NW. Pharmacological analysis of directionally sensitive rabbit retinal ganglion cells. J Physiol (Lond). 1982; 324:161–185. [PubMed: 7097594]
7. Kittila CA, Massey SC. Effect of ON pathway blockade on directional selectivity in the rabbit retina. J Neurophysiol. 1995; 73:703–712. [PubMed: 7760129]
8. Weng S, Sun W, He S. Identification of ON-OFF direction-selective ganglion cells in the mouse retina. J Physiol (Lond). 2005; 562:915–923. [PubMed: 15564281]
9. Famiglietti EV. Synaptic organization of starburst amacrine cells in rabbit retina: analysis of serial thin sections by electron microscopy and graphic reconstruction. J Comp Neurol. 1991; 309:40–70. [PubMed: 1894768]
10. Stacy RC, Wong RO. Developmental relationship between cholinergic amacrine cell processes and ganglion cell dendrites of the mouse retina. J Comp Neurol. 2003; 456:154–166. [PubMed: 12509872]
11. Yoshida K, et al. A key role of starburst amacrine cells in originating retinal directional selectivity and optokinetic eye movement. Neuron. 2001; 30:771–780. [PubMed: 11430810]
12. Amthor FR, Keyser KT, Dmitrieva NA. Effects of the destruction of starburst-cholinergic amacrine cells by the toxin AF64A on rabbit retinal directional selectivity. Vis Neurosci. 2002; 19:495–509. [PubMed: 12511082]
13. Chen YC, Chiao CC. Symmetric synaptic patterns between starburst amacrine cells and direction selective ganglion cells in the rabbit retina. J Comp Neurol. 2008; 508:175–183. [PubMed: 18306383]
14. Famiglietti EV. A structural basis for omnidirectional connections between starburst amacrine cells and directionally selective ganglion cells in rabbit retina, with associated bipolar cells. Vis Neurosci. 2002; 19:145–162. [PubMed: 12385627]
15. Jeon CJ, et al. Pattern of synaptic excitation and inhibition upon direction-selective retinal ganglion cells. J Comp Neurol. 2002; 449:195–205. [PubMed: 12115689]

16. Chan YC, Chiao CC. Effect of visual experience on the maturation of ON-OFF direction selective ganglion cells in the rabbit retina. Vision Res. 2008; 48:2466–2475. [PubMed: 18782584]
17. Chen M, Weng S, Deng Q, Xu Z, He S. Physiological properties of direction-selective ganglion cells in early postnatal and adult mouse retina. J Physiol (Lond). 2009; 587:819–828. [PubMed: 19103682]
18. Elstrott J, et al. Direction selectivity in the retina is established independent of visual experience and cholinergic retinal waves. Neuron. 2008; 58:499–506. [PubMed: 18498732]
19. Huberman AD, et al. Genetic identification of an On-Off direction-selective retinal ganglion cell subtype reveals a layer-specific subcortical map of posterior motion. Neuron. 2009; 62:327–334. [PubMed: 19447089]
20. Watanabe D, et al. Ablation of cerebellar Golgi cells disrupts synaptic integration involving GABA inhibition and NMDA receptor activation in motor coordination. Cell. 1998; 95:17–27. [PubMed: 9778244]
21. Togashi H, et al. Cadherin regulates dendritic spine morphogenesis. Neuron. 2002; 35:77–89. [PubMed: 12123610]
22. Zhu H, Luo L. Diverse functions of N-cadherin in dendritic and axonal terminal arborization of olfactory projection neurons. Neuron. 2004; 42:63–75. [PubMed: 15066265]
23. Dong W, Sun W, Zhang Y, Chen X, He S. Dendritic relationship between starburst amacrine cells and direction-selective ganglion cells in the rabbit retina. J Physiol (Lond). 2004; 556:11–17. [PubMed: 14978206]
24. Vaney, DI.; Collin, SP.; Young, HM. Neurobiology Of The Inner Retina. Weiler, R.; Osborne, NN., editors. Springer; 1989.
25. Elstrott J, Feller MB. Direction-selective ganglion cells show symmetric participation in retinal waves during development. J Neurosci. 2010; 30:11197–11201. [PubMed: 20720127]
26. Wang CT, et al. GABA(A) receptor-mediated signaling alters the structure of spontaneous activity in the developing retina. J Neurosci. 2007; 27:9130–9140. [PubMed: 17715349]
27. Huang ZJ. Activity-dependent development of inhibitory synapses and innervation pattern: role of GABA signalling and beyond. J Physiol (Lond). 2009; 587:1881–1888. [PubMed: 19188247]
28. Petreanu L, Mao T, Sternson SM, Svoboda K. The subcellular organization of neocortical excitatory connections. Nature. 2009; 457:1142–1145. [PubMed: 19151697]
29. Li Y, Van Hooser SD, Mazurek M, White LE, Fitzpatrick D. Experience with moving visual stimuli drives the early development of cortical direction selectivity. Nature. 2008; 456:952–956. [PubMed: 18946471]
30. Wei W, Elstrott J, Feller MB. Two-photon targeted recording of GFP-expressing neurons for light responses and live-cell imaging in the mouse retina. Nature Protocols. 2010; 5:1347–1352.

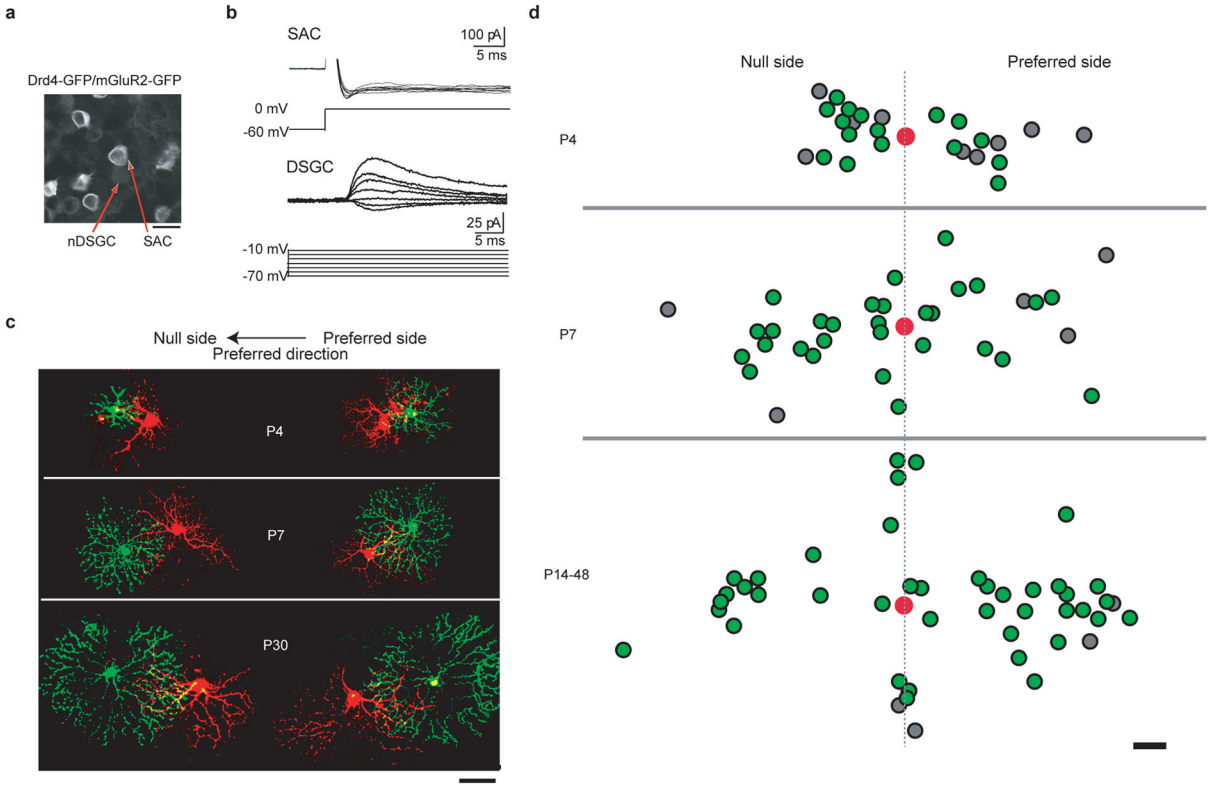

Figure 1. nDSGCs receive direct GABAergic inputs from SACs located on the null and the preferred side from P4 until adult

a, Fluorescence image of the ganglion cell layer from a P30 *Drd4–GFP/mGluR2–GFP* mouse, showing the bright membrane-bound GFP expressed under the *mGluR2* promoter in the SACs and the dim cytoplasmic GFP driven by the *Drd4* promoter in the nDSGC. Scale bar, 25 μm. **b**, Paired whole-cell voltage-clamp recordings of GABAergic currents in a P4 nDSGC (lower traces) evoked by depolarization of a SAC from the null side (upper traces) in the presence of the NMDA (*N*-methyl-D-aspartate) receptor antagonist D(−)-2-amino-5-phosphonovaleric acid (AP5), α-amino-3-hydroxy-5-methyl-4-isoxazole propionic acid (AMPA)/kainate receptor antagonist 6,7-dinitroquinoxaline-2,3-dione (DNQX) and α4-containing nicotinic acetylcholine receptor antagonist dihydro-β-erythroidine (DHβE). SACs were depolarized from −60 to 0 mV, which reliably evoked an inward current in SACs. The postsynaptic GABAergic currents were recorded in DSGCs at different holding potentials to determine the current–voltage relationship of the conductance. **c**, Example images of synaptically connected, dye-filled SAC–DSGC pairs at P4, P7 and P30. The left-hand side shows pairs with SACs (green) located on the null side of the DSGCs (red). The right-hand side shows preferred-side pairs. Scale bar, 50 μm. **d**, Soma locations of the GABAergically connected SAC–nDSGC pairs along the null-preferred axis during development. Red spots represent the positions of DSGC cell bodies. The positions of SAC cell bodies that form GABAergic synapses with their respective nDSGCs are shown as green spots; the SAC cell bodies that were not connected to nDSGCs are shown as grey spots. All pairs had overlapping dendritic fields. Scale bar, 25 μm

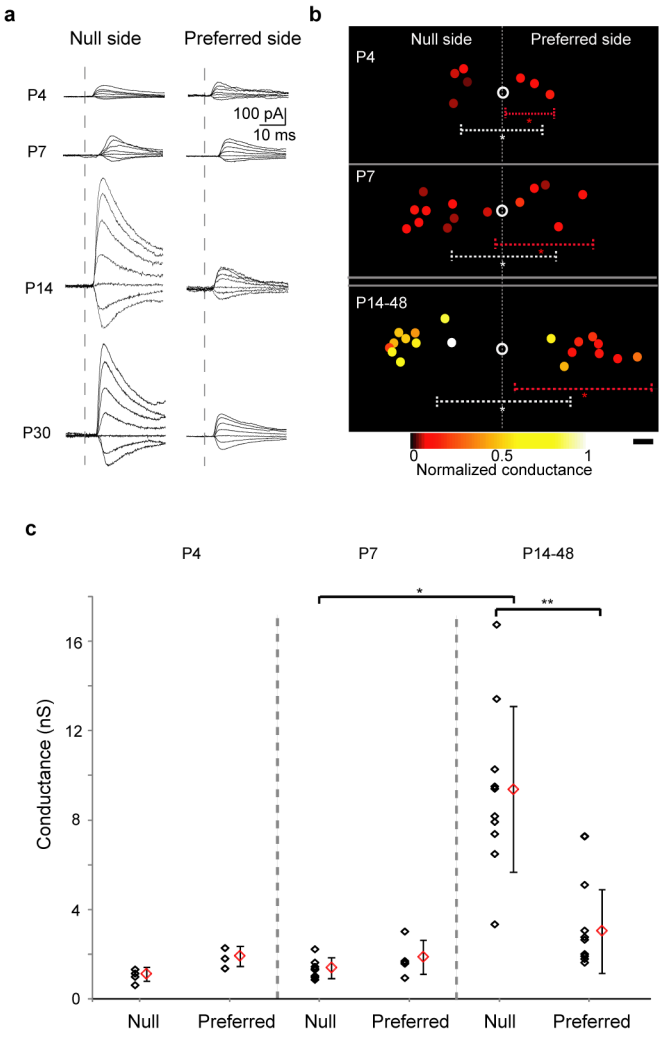

Figure 2. GABAergic conductance in the null-side SAC–nDSGC pairs strengthens during the second postnatal week

a, Postsynaptic GABAergic currents in nDSGCs recorded at holding potentials between −70 and −10 mV in response to depolarization (as in Fig. 1b) of null-side (left) and preferred-side (right) SACs at P4, P7, P14 and P30. **b**, Relative soma positions of SAC–nDSGC pairs used for conductance analysis at P4, P7 and P14–48. Open circles represent nDSGC cell bodies. Filled circles are SAC somas colour-coded for conductance strength normalized to the maximum value across all ages. Dashed lines illustrate average dendritic arborization diameter, centred on the asterisks, for nDSGCs (white) and SACs (red; asterisks represent average soma locations). Scale bar, 25 μm. **c**, Summary plot of GABAergic conductances of the null- and preferred-side SAC–nDSGC pairs at P4, P7 and P14–48. Individual pairs and mean ± s.d. are shown. One-way analysis of variance: $P < 0.0001$; *t*-test: $*P < 0.0001$, $**P = 0.0003$.

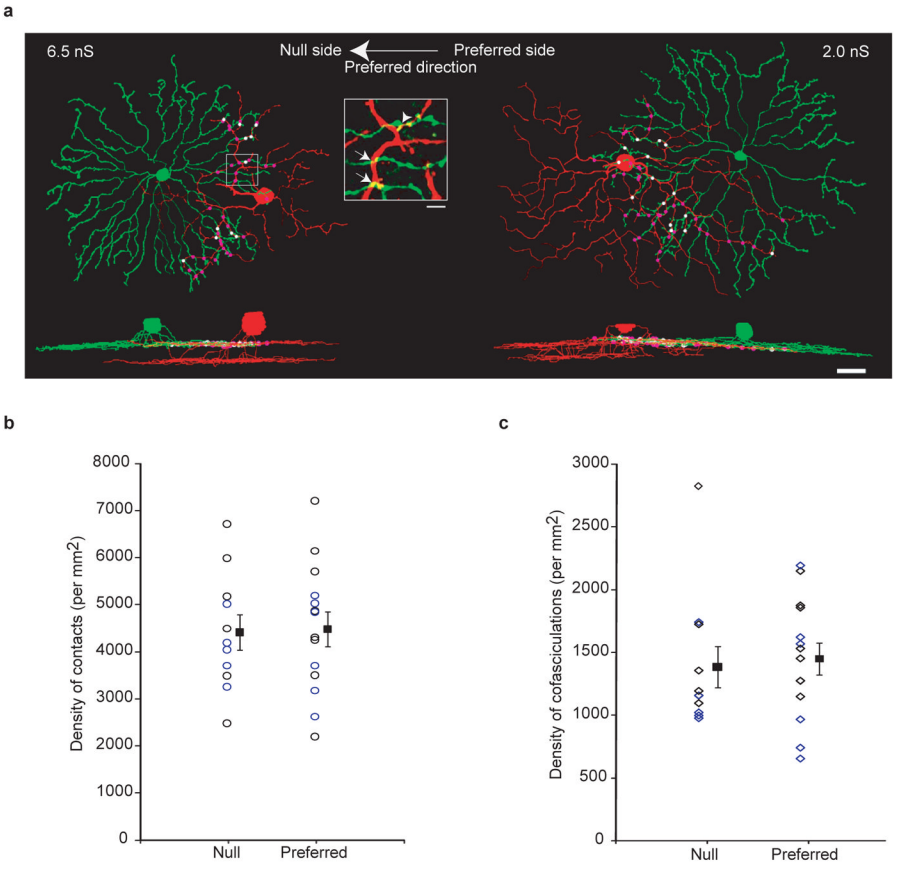

Figure 3. Dendritic contacts and cofasciculations between SACs and nDSGCs occur at similar densities for the null- and preferred-side pairs

a, NEUROLUCIDA reconstructions of the dendrites from the on sublamina and side views of the complete dendritic arborizations from a null-side (left) and a preferred-side (right) pair of SACs and nDSGCs. Dots represent dendritic contacts, with cofasciculation segments coloured white and the rest coloured purple. The GABAergic conductances for the null- and preferred-side pairs are indicated. Scale bar, 25 μm. Inset, fluorescence image of the outlined region showing crossing contacts (arrows) and cofasciculation (arrowhead). Scale bar, 5 μm. **b**, Summary plot of the density of total contacts between DSGCs and distal SAC processes (roughly the outer third) from the null or preferred side from P14 to P48. Individual pairs and mean ± s.d. are shown. The data points for P28 and later are coloured blue, and the ones for before P28 are coloured black. **c**, Summary plot of the density of cofasciculations between nDSGCs and distal SAC processes from the same pairs as in **b**. Null- and preferred-side groups are not significantly different in **b** and **c**. $P > 0.7$, *t*-test.

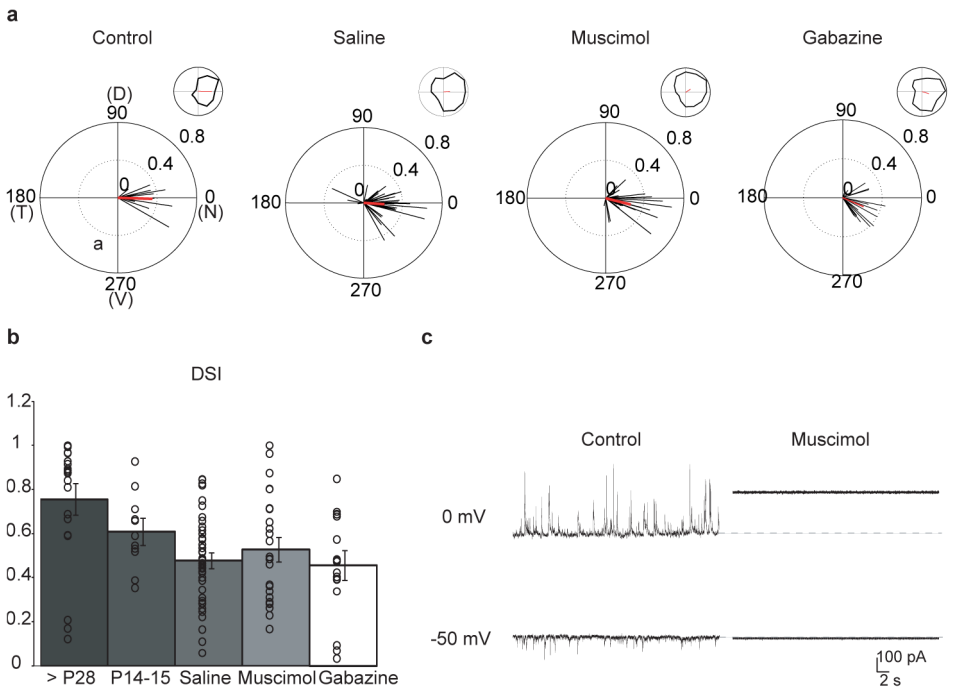

Figure 4. Intraocular injections of muscimol or gabazine do not alter direction selectivity in nDSGCs

a, The normalized spike vector sums of nDSGCs in response to drifting gratings of 12 directions from P14–15 *Drd4–GFP* mice that received either no treatment (control) or intraocular injections of saline, muscimol or gabazine from P6 to P12. D, dorsal; N, nasal; T, temporal; V, ventral. The red lines are mean vector sums of all cells in each group. Insets, examples of normalized tuning curves of single cells, with corresponding vector sums represented as red lines of nDSGCs from each group. Control: n = 4 mice, 12 cells; saline: n = 11 mice, 43 cells; muscimol: n = 12 mice, 25 cells; gabazine: n = 4 mice, 17 cells. **b**, Summary plot of direction selectivity index (DSI) for adult (>P28), P14–15 untreated, saline, muscimol and gabazine-treated groups. Bars show mean ± s.e.; open circles represent individual cells. Adult data are reproduced from ref. 19. **c**, Example traces from whole-cell voltage-clamp recordings of inhibitory (upper traces, V_H = 0 mV) and excitatory (lower traces, V_H = −50 mV) currents from a P14 nDSGC in drug-free artificial cerebrospinal fluid (control, left) or artificial cerebrospinal fluid containing 100 μM muscimol (right). Deflections from baseline correspond to spontaneous synaptic currents. At depolarized potentials, application of muscimol activated a tonic current, which was measured as a change in the baseline holding current[26].